Features critical for membrane binding revealed by DivIVA crystal structure

Maria A Oliva[1,4], Sven Halbedel[2,4], Stefan M Freund[3], Pavel Dutow[2], Thomas A Leonard[1,5], Dmitry B Veprintsev[1], Leendert W Hamoen[2,*] and Jan Löwe[1,*]

[1]MRC Laboratory of Molecular Biology, Cambridge, UK, [2]Center for Bacterial Cell Biology, Institute for Cell and Molecular Biosciences, Newcastle University, Framlington Place, Newcastle upon Tyne, UK and [3]MRC Centre for Protein Engineering, Cambridge, UK

DivIVA is a conserved protein in Gram-positive bacteria that localizes at the poles and division sites, presumably through direct sensing of membrane curvature. DivIVA functions as a scaffold and is vital for septum site selection during vegetative growth and chromosome anchoring during sporulation. DivIVA deletion causes filamentous growth in *Bacillus subtilis*, whereas overexpression causes hyphal branching in *Streptomyces coelicolor*. We have determined the crystal structure of the N-terminal (Nt) domain of DivIVA, and show that it forms a parallel coiled-coil. It is capped with two unique crossed and intertwined loops, exposing hydrophobic and positively charged residues that we show here are essential for membrane binding. An intragenic suppressor introducing a positive charge restores membrane binding after mutating the hydrophobic residues. We propose that the hydrophobic residues insert into the membrane and that the positively charged residues bind to the membrane surface. A low-resolution crystal structure of the C-terminal (Ct) domain displays a curved tetramer made from two parallel coiled-coils. The Nt and Ct parts were then merged into a model of the full length, 30 nm long DivIVA protein.

*Corresponding authors. LW Hamoen, The Centre for Bacterial Cell Biology, Medical Science New Building, Medical School, Newcastle University, Richardson Road, Newcastle upon Tyne NE2 4AX, UK. Tel.: +44 191 208 3240; Fax: +44 191 222 7424;
E-mail: l.hamoen@ncl.ac.uk or J Löwe, MRC Laboratory of Molecular Biology, Hills Road, Cambridge CB2 2QH, UK. Tel.: +44 1223 252969; Fax: +44 1223 213556; E-mail: jyl@mrc-lmb.cam.ac.uk
[4]These authors contributed equally to this work
[5]Present address: Laboratory of Molecular Biology, NIDDK, National Institutes of Health, 9000 Rockville Pike, Building 5, Room 405, Bethesda, MD 20892-0580, USA

Received: 15 January 2010; accepted: 22 April 2010

Introduction

Many proteins in rod-shaped bacteria are confined to the cell pole, which can therefore be considered a specialized compartment. However, there is no physical barrier that separates the polar region from the rest of the cell, and there is no dedicated machinery known that transports proteins to this area. The mechanism of polar localization in bacteria has remained elusive until very recently when it was shown that the curvature of the cell membrane is one of the characteristics that can be used by proteins to detect the extremities of the cell. For rod-shaped cells, the curvature of the cell membrane is not homogenous, and at cell division sites and cell poles, the membrane surface is more strongly bent having spherical instead of cylindrical curvature (although still weakly in absolute terms). The DivIVA protein appears to be able to recognize membranes that are curved inwards (negative curvature), and therefore accumulates at cell poles, and as a ring-like structure at the division septum where greater negative curvature exists as well (Lenarcic *et al*, 2009; Ramamurthi and Losick, 2009). DivIVA is the first bacterial protein for which it has been shown that negative membrane curvature can function as a topological marker. Because of a lack of structural information, the exact molecular mechanism of DivIVA localization has remained unknown.
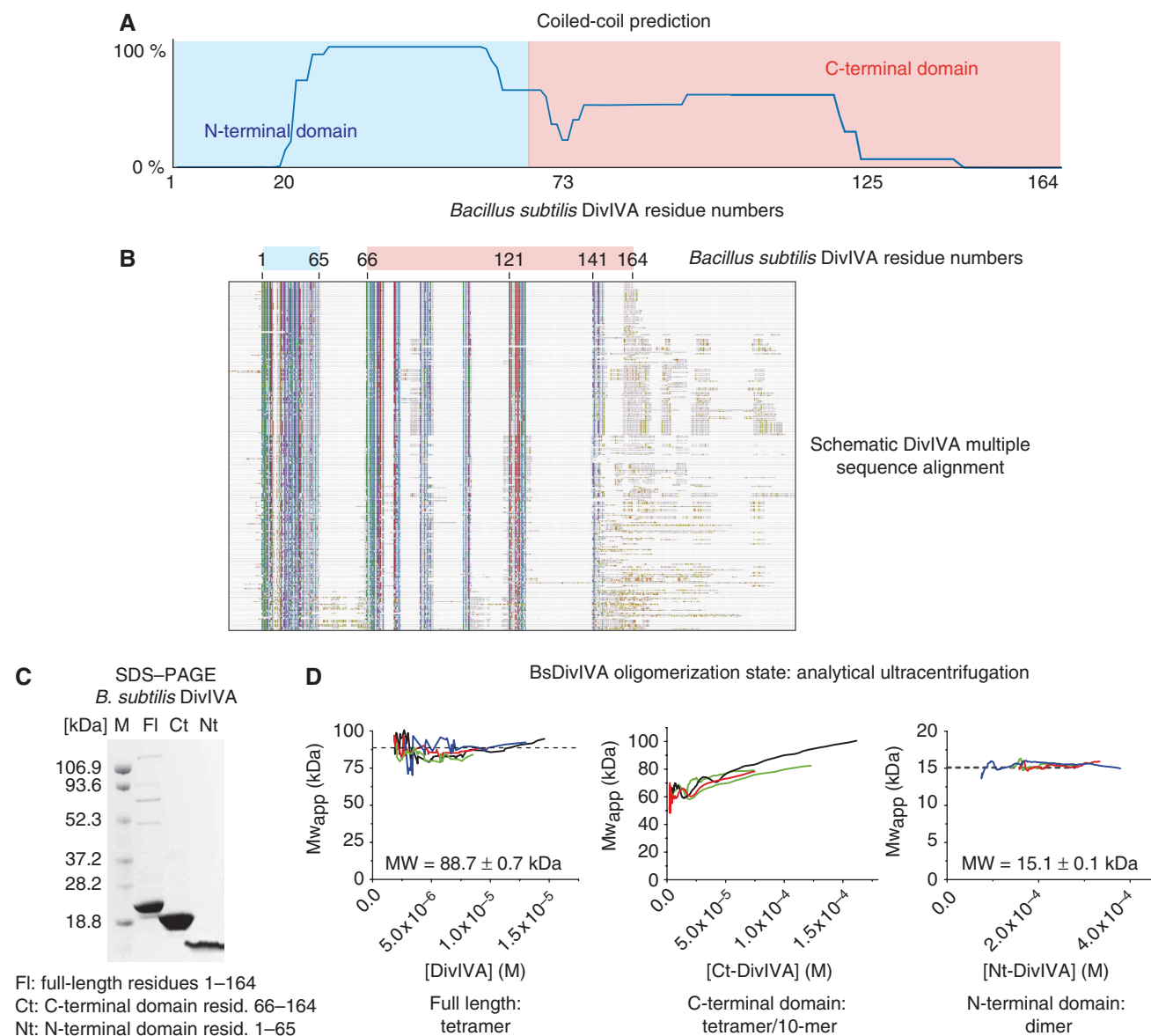
DivIVA is highly conserved in Gram-positive bacteria. It is involved in many different processes, and functions as a scaffold for proteins that require localization at the cell division site and/or cell poles. The characteristic localization pattern of DivIVA was first observed in *Bacillus subtilis*. In this organism, the protein is responsible for polar localization of the division inhibitor MinC/MinD that prevents polymerization of FtsZ close to cell poles (Edwards and Errington, 1997; Marston *et al*, 1998; Gregory *et al*, 2008). Mutations in *divIVA* result in delocalization of MinC and MinD, and as a consequence, cells can divide aberrantly close to cell poles, producing small anucleate minicells. DivIVA also has an important function during sporulation. Incorporation of DNA into the polar pre-spore compartment is achieved by anchoring one chromosome copy to the distal pole of the pre-spore compartment. One of the proteins involved in this process is RacA, and DivIVA is responsible for its polar localization (Ben-Yehuda *et al*, 2003; Wu and Errington, 2003). Gram-positive cocci such as *Streptococcus pneumoniae* and *Staphylococcus aureus* also contain a DivIVA homologue, although these bacteria do not contain a MinC/MinD system and do not sporulate. In *S. pneumoniae*, deletion of *divIVA* results in a severe cell division defect, and two-hybrid experiments suggested that DivIVA interacts with a number of cell division proteins (Fadda *et al*, 2003). In *Streptomyces coelicolor*, DivIVA has an important role in tip growth and branching (Flärdh, 2003; Hempel *et al*, 2008), and it was suggested that a cellulose-synthase-like protein, involved in tip growth, may interact with DivIVA (Xu *et al*, 2008).

A Coiled-coil prediction

B *Bacillus subtilis* DivIVA residue numbers

Schematic DivIVA multiple sequence alignment

C SDS–PAGE
B. subtilis DivIVA

Fl: full-length residues 1–164
Ct: C-terminal domain resid. 66–164
Nt: N-terminal domain resid. 1–65

D BsDivIVA oligomerization state: analytical ultracentrifugation

Full length: tetramer — MW = 88.7 ± 0.7 kDa

C-terminal domain: tetramer/10-mer

N-terminal domain: dimer — MW = 15.1 ± 0.1 kDa

Figure 1 *B. subtilis* DivIVA can be divided into two domains. (**A**) Coiled-coil prediction of *B. subtilis* DivIVA (Lupas *et al*, 1991). The protein contains two dominant coiled-coil segments and short, non-coiled segments at each end. (**B**) Schematic multiple sequence alignment showing the exact domain boundaries chosen based on the first insertion (after residue 65, *B. subtilis* numbering). The database was queried using *B. subtilis* DivIVA and BLAST and the 250 highest scoring sequences related to BsDivIVA were aligned using ClustalW (Thompson *et al*, 1994). The figure shows the resulting multiple sequence alignment schematically, each amino acid coloured according to conservation and types of residues conserved (ClustalX colour scheme). *B. subtilis* DivIVA is the first sequence and the sequence numbering is shown above, highlighting the domain boundaries (blue: N-terminal domain, red: C-terminal domain). (**C**) Coomassie-stained SDS–PAGE showing purified *B. subtilis* DivIVA full-length and the N- and C-terminal domains. (**D**) Sedimentation-equilibrium analytical ultracentrifugation experiments of full-length DivIVA and the N- and C-terminal domains. Full-length protein is a tetramer, although some non-reversible aggregation also occurred. The C-terminal domain is a tetramer mixed with decamers and the N-terminal domain is a dimer. For each protein, four independent centrifugation cells are plotted in different colours.

B. subtilis DivIVA protein comprises 164 amino acids and is predicted to be largely α-helical and coiled-coil (Figure 1A), a general feature of all DivIVA proteins. The protein in a mutant form has been reported to form oligomers composed of 6–8 monomers (Stahlberg *et al*, 2004). Electron microscopy showed that these oligomers form large 'bone-like' structures with a length of about 22 nm. The ends of these structures appear to interact with each other to form oligomers. A deletion analysis has shown that the lipid targeting domain is confined to the N-terminal (Nt) domain of the protein, and based on site-directed mutagenesis, it was suggested that an

amphipathic helix, spanning amino acids 22–41, might insert into the lipid bilayer (Lenarcic *et al*, 2009). Similar domain assignments have recently been proposed for DivIVA from *Streptomyces* and *Corynebacterium* (Letek *et al*, 2009; Wang *et al*, 2009). Another study identified amino acids 17, 18 and 19 (*B. subtilis* DivIVA) as important for polar localization of DivIVA (Perry and Edwards, 2004).

The need for structural data on DivIVA is apparent, and we set out to crystallize *B. subtilis* DivIVA. Eventually, this was possible by dividing the protein into an Nt and C-terminal (Ct) domain as suggested by an earlier study (Lenarcic *et al*,

2009). The composite model of DivIVA, containing the Nt and Ct domains, shows a predominantly coiled-coil structure, 30 nm long when fully extended. The crystal structure of the Nt domain reveals a unique crossed-loop structure that exposes two phenylalanines to the solvent. Extensive site-directed mutagenesis of this domain and a suppressor screen showed that this hydrophobic residue together with positively charged amino acids is responsible for membrane binding.

Results

B. subtilis DivIVA protein can be divided into two domains

Our many attempts to determine the structure of full-length DivIVA proteins from a number of different organisms failed due to a lack of diffraction quality crystals. To move forward, we decided to investigate the protein as individual domains. For *B. subtilis* DivIVA, the subject of this study, we divided the protein into two domains, Nt and Ct, inspired by an earlier study (Lenarcic *et al*, 2009). The exact boundaries were defined based on the coiled-coil prediction (Figure 1A) and a comprehensive multiple sequence alignment, seeded with *B. subtilis* DivIVA (Figure 1B). The coiled-coil prediction shows two clear coiled-coil segments and non-coiled segments of 20–30 residues, one at each end. The multiple sequence alignment indicates that the domain boundary occurs after the first coiled-coil segment (after residue 65). The Ct domain has more insertions and some DivIVA sequences have long Ct tails that do not align. Overall sequence conservation is high, certainly for a coiled-coil protein, with the highest conservation being located within the Nt domain (Figure 1B).

We expressed the two domains and the full-length DivIVA protein in *Escherichia coli* and they are well behaved and can be purified to high purity (Figure 1C). The individual domains comprise residues 1–65 and 66–164 for the Nt and Ct domains, respectively.

To get an idea of the oligomerization state of the individual domains when compared with the full-length protein, we performed analytical ultracentrifugation experiments (Figure 1D). Using a sedimentation-equilibrium setup, we determined that full-length *B. subtilis* DivIVA is a mix of tetramers and a small minority of precipitating aggregates (Figure 1D, left), similar to what has been reported for a mutant protein before (Stahlberg *et al*, 2004). The Ct domain still forms tetramers and something that appears to be 10-mers (Figure 1D, middle). The Nt domain forms a very clear and well-defined dimer (Figure 1D, right).

High-resolution structure of the Nt domain reveals a crossed dimer

Initially, it proved impossible to obtain crystals of the Nt domain of *B. subtilis* DivIVA (residues 1–65). An NMR HSQC experiment showed that the protein is folded (Figure 2A). Further experiments, leading to a full assignment (Figure 2A and B), highlighted that the protein contains two helical segments (from residues 6 to 9 and from residues 21 to 57). Moreover, they showed that the last residues have greater mobility and are not folded into a rigid structure. When these residues where removed from the protein (NtDivIVA-2, residues 1–57, no tag), crystals could be obtained that diffracted to high
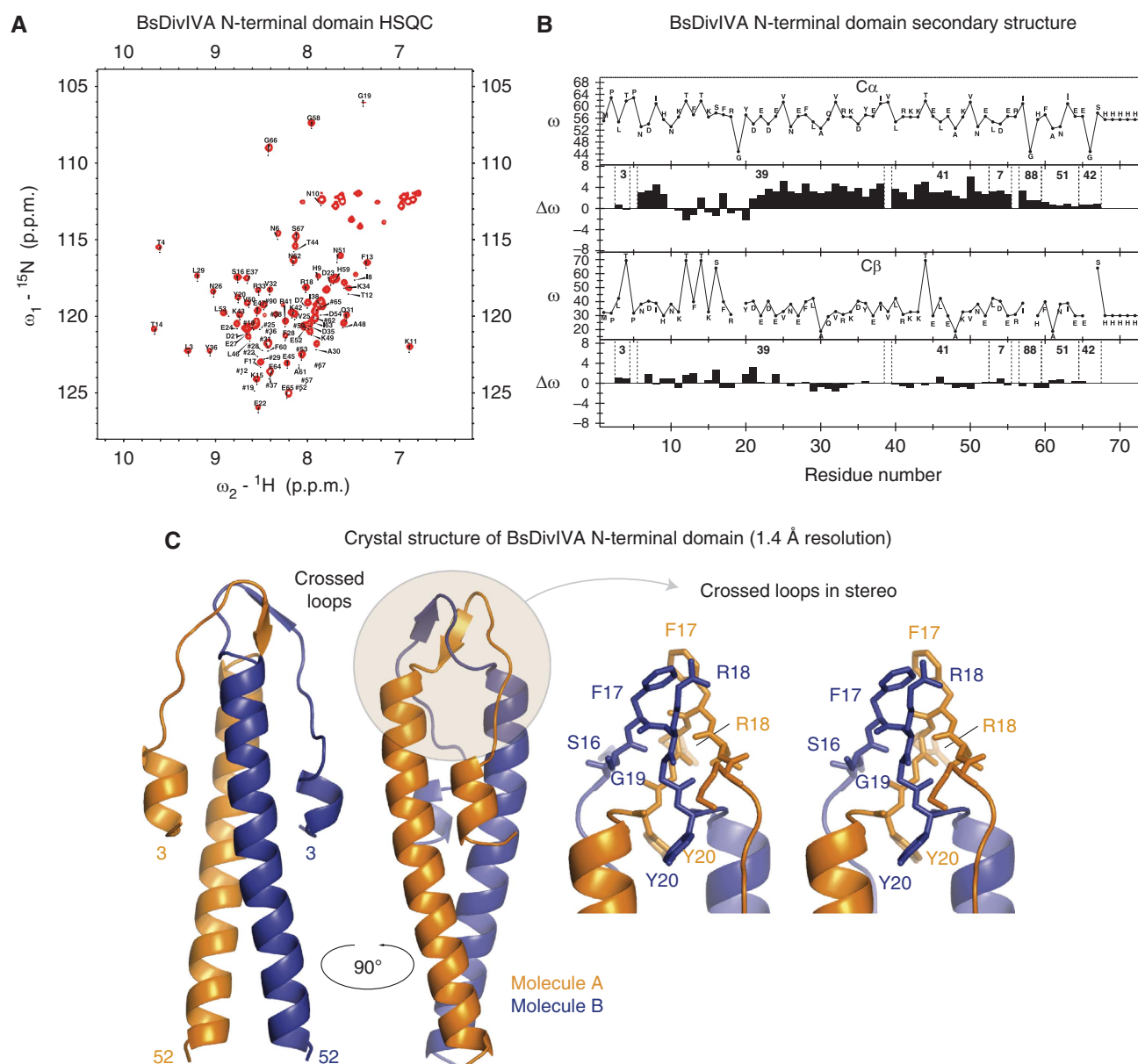
resolution (Table I). The structure was solved using a quick sodium iodide soak and an in-house, off-edge iodide SAD experiment.

The Nt domain of DivIVA is a coiled-coil dimer (Figure 2C). The coiled-coil helices are arranged in parallel, matching the arrangement of the structure of the Ct domain as described later (Figure 5D). Residues 3–22 form a short helical segment and a longer loop. To our surprise, the two loops from the two molecules in the dimer crossover and are intimately intertwined. This peculiar structure exposes F17 and R18 from both chains to the outside solvent (Figure 2C, right). Exposure is surprising for phenylalanine residues, in particular for two in proximity, which are not normally exposed on the surface of proteins due to their hydrophobicity.

Mutagenic analysis of residues in the Nt domain reveals their importance for localization

Mutagenesis and *in vivo* analysis was performed on the residues that where highlighted by the structure of the Nt domain (Supplementary Table S5). Amino acids that were found to be conserved or similar, according to a sequence alignment involving DivIVA proteins from different Firmicutes (Figure 3A), were changed to alanine or glycine. All mutant variants were expressed as *Pspac-divIVA* constructs from the *aprE* locus in a strain in which the native *divIVA* gene was replaced by a tetracyclin resistance cassette. As can be seen in Figure 3B (left), replacement of *divIVA* leads to the typical filamentous growth of a *B. subtilis* Δ*divIVA* mutant (Edwards and Errington, 1997). Ectopic expression of a wild-type copy of *divIVA* produces cells that display normal cell lengths, indicating that this copy functionally complements an endogenous *divIVA* replacement. This was also seen when sporulation of these strains was analysed using a simple plate assay (Figure 3B, right). The Δ*divIVA* mutant did not sporulate at all, but its sporulation was restored to wild-type level when the ectopic *divIVA* gene was present. In contrast to this, *divIVA* null phenotypes were observed when I8A, F13A, F17G, F17A, R18A, G19A, V25A, F28A and L29A variants of *divIVA* were analysed for their potential to restore vegetative growth or sporulation of the Δ*divIVA* mutant (Figure 3B). This suggests that these mutations lead to inactive or mistargeted DivIVA proteins. In contrast to the results obtained with these mutants, no or only mild effects on DivIVA activity were observed in case of K11A, S16G, Y20A, D21A, E24A, V32A, D35A, E37A and V39A.

Since localization to the poles and the division site is one important prerequisite for proper DivIVA function, we hypothesized that mutations in the Nt domain would interfere with the targeting of DivIVA to the cytoplasmic membrane. To test this hypothesis, the same set of mutations was introduced into *divIVA-gfp*. These mutant variants were ectopically expressed as *Pxyl-divIVA-gfp* constructs from the *amyE* locus and combined with the Δ*divIVA* background, ensuring that the mutated DivIVA-GFP proteins could not interact with endogenous DivIVA through dimerization or oligomerization. When localization of wild-type DivIVA-GFP was analysed in such an experiment, polar dots and bright bands at cell division sites were observed (Figure 3C), representing the normal subcellular distribution of DivIVA. Expression of DivIVA-GFP in the Δ*divIVA* mutant did not restore wild-type division and sporulation (data not shown), in agreement with

A BsDivIVA N-terminal domain HSQC

B BsDivIVA N-terminal domain secondary structure

C Crystal structure of BsDivIVA N-terminal domain (1.4 Å resolution)

Molecule A
Molecule B

Figure 2 High-resolution X-ray crystal structure of the N-terminal domain of DivIVA. (**A**) NMR HSQC spectrum of the initial DivIVA N-terminal domain construct (1–65). Full assignment is shown. (**B**) Summary of NMR backbone dynamics showing secondary structure elements and also that some residues at the C-terminal end are not ordered. These were then removed producing a new construct (1–57) that was crystallized. (**C**) Left: 1.4 Å resolution X-ray crystal structure of the N-terminal domain (1–57) of DivIVA. The protein forms a parallel coiled-coil dimer and also contains another small helix that binds to the sides of the coiled-coil. This arrangement produces a crossed-loop structure on the top (right), with several residues being very exposed to the solvent (residues 16–19). Most striking is exposure of the two hydrophobic phenylalanine residues F17 to the outside.

earlier reports that a DivIVA-GFP fusion is not functional (Edwards and Errington, 1997). The patterns of localization observed with the inactive Nt domain mutants fell into different classes (Figure 3C): I8A, F13A, V25A, F28A, L29A amino acid changes gave rise to the formation of bright foci, probably representing inclusion bodies formed by misfolded DivIVA-GFP. In contrast, F17G, F17A and G19A resulted in diffuse proteins, whereas R18A caused accumulation in cytoplasmic spots. All other mutant proteins displayed normal (S16G, D21A, E37A) or intermediate (K11A, E22G, E24A, V32A, D35A V39A) localization patterns (Supplementary Table S5).

To better understand the mutagenesis results, we projected the amino acid mutations onto the crystal structure. As shown in Figure 4A, all but three of the null mutants causing filamentous growth and mislocalization are located within the core of the Nt domain structure. Most likely, these mutants affect the proper folding of the N-terminus. That they do disrupt more than just membrane targeting can be seen from the loss of DivIVA self-interaction in Figure 3D for all of them, except F17G. One of the three exceptions is G19A, which is probably another folding mutant because of the stereochemical uniqueness of glycine. Importantly, the two other, F17 and R18, are part of the crossed-loop structure

Table I Crystallographic data

Protein	Ct SeMet hexagonal CtDivIVA-I114M-His$_6$	Ct TABR tetragonal CtDivIVA-His$_6$	NtDivIVA nati NtDivIVA-2	Nt NaI deri NtDivIVA-2	Nt F17A mutant Nt-2-F17A
Data					
Space group	P6$_2$22	P4$_1$22	P2$_1$2$_1$2$_1$	P2$_1$2$_1$2$_1$	P2$_1$
Cell dimensions					
a (Å)	210.8	133.5	29.1	29.1	57.7
b (Å)	210.8	133.5	32.8	32.9	28.7
c (Å)	60.4	181.3	134.5	141.5	66.2
α (deg)	90.0	90.0	90.0	90.0	90.0
β (deg)	90.0	90.0	90.0	90.0	105.9
γ (deg)	90.0	90.0	90.0	90.0	90.0
Resolution (Å)	6.00	7.00	1.40	2.60	1.90
R_{sym}	0.145	0.081	0.069	0.064	0.053
I/σ (I)	18.7	22.4	11.2	17.5	13.3
Completeness (%)[a]	99.9 (100.0)	99.4 (100.0)	94.5 (88.7)	96.7 (84.6)	96.7 (95.0)
Redundancy	37.0 (ano. 21.7)	24.1 (ano. 14.1)	3.8	4.3 (ano. 2.5)	2.8
Phasing	Se SAD	Ta SAD	MR	I SAD	MR
Number of sites	6	5		8	
Mean FOM	0.306	0.400		0.478	
Refinement					
R_{work}[a]			0.186 (0.228)		0.159 (0.243)
R_{free}[a,b]			0.222 (0.265)		0.240 (0.327)
No. of atoms			1067		2242
Protein			856		1854
Water			211		388
B-factors (Å^2)[c]			23.8		16.85
r.m.s. deviation					
Bond lengths (Å)			0.031		0.007
Bond angles (deg)			2.599		0.949
B-factors			1.42		4.25
Model					
Molecules per asu	2	6	2	2	4
Solvent content (%)	83.0	75.0	47.6		36.2
Ramachandran[d] (%)			97.8 (0.0)		98.5 (0.0)
PDB ID			2WUJ		2WUK

[a]Values in parentheses are for the highest resolution shell.
[b]For determination of R_{free}, 5% of reflections were randomly selected before refinement.
[c]Temperature factors averaged for all atoms and r.m.s. deviation of temperature factors between bonded atoms.
[d]Percentage of residues in the 'most favoured region' of Ramachandran plot and percentage of outliers.

(see Figure 2C, right) and the side chains of those two residues are clearly exposed on the surface of the protein, with all other null mutant side chains being located inside. In contrast, all milder mutants are located on the surface and probably do not affect folding (Figure 4A, right).

To exclude misfolding of the Nt crossed-loop structure by replacing F17, we purified the Nt domain with a F17A mutation, crystallized the protein and solved the structure by molecular replacement (Figure 4B; Table I). Satisfyingly, the resulting structure shows no major changes and the crossed-loop structure is still intact, without the two exposed phenylalanine residues.

Phenylalanine 17 is essential for membrane binding
As mutations of F17 result in a cytoplasmic localization of the DivIVA-GFP fusion (Figure 3C), and due to the hydrophobic nature of phenylalanine, this residue might be crucial for membrane interaction. To test this, we purified the F17A mutant and investigated membrane binding *in vitro*. Wild-type DivIVA binds to lipid vesicles, and in a spin assay, the protein is pelleted together with the liposomes, as shown in Figure 4C. When the same experiment was repeated with the F17A mutant, no protein was detected in the pellet
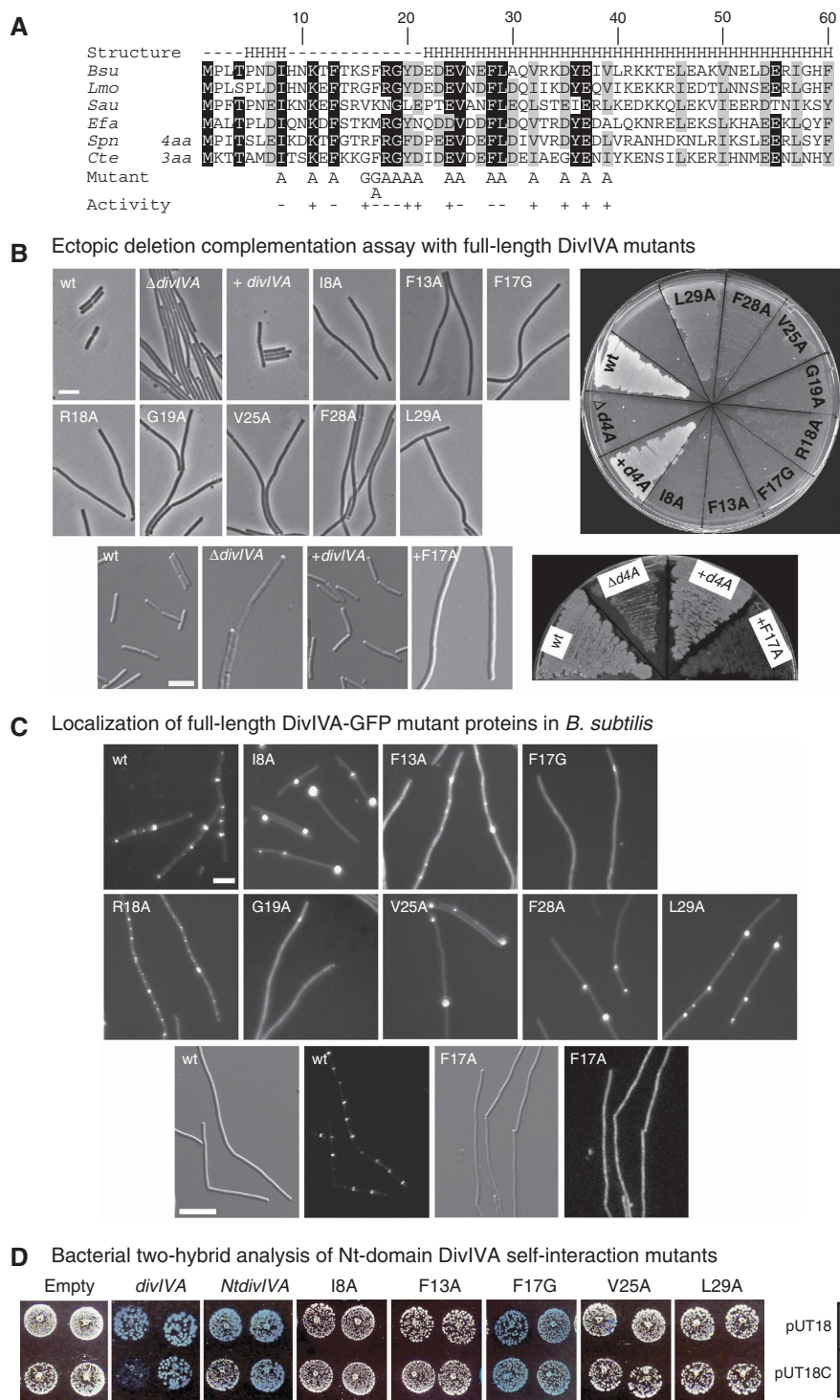
(Figure 4C). As shown above, the F17A mutant does not affect folding of the protein, thus we can conclude that F17 is essential for membrane binding.

### Suppressor mutation indicates the importance of positive charges for membrane binding
The F17G and F17A substitutions are fairly drastic alterations. Interestingly, even if we replaced F17 by the other hydrophobic amino acids methionine, valine or leucine, the localization of the respective mutated DivIVA-GFP fusion was still disturbed (data not shown and Figure 4D, middle). The relatively mild alteration in the F17V mutant provided an opportunity to screen for suppressor mutations. The F17V mutation also abolished sporulation, which is an easily selectable phenotype (Figure 4D, bottom). To reduce false positives, we included the *divIVAF17V-GFP* fusion, so that we could conveniently test suppressors for restored localization. The motivation for such screen was that suppressors of the F17V mutant could reveal other proteins involved in DivIVA localization.

For screening, strain BSN54 was constructed that contains a deletion in *divIVA* and a *Pspac-divIVAF17V* allele and *Pxyl-divIVAF17V-gfp* expressed from the *aprE* and *amyE* locus,

A

B Ectopic deletion complementation assay with full-length DivIVA mutants

C Localization of full-length DivIVA-GFP mutant proteins in *B. subtilis*

D Bacterial two-hybrid analysis of Nt-domain DivIVA self-interaction mutants

Figure 3 Mutational analysis of the N-terminal domain of DivIVA. (**A**) Alignment of the DivIVA N-terminal domain sequences from different Firmicutes. Amino acids with >80% identity or similarity are black boxed or grey shaded, respectively. The secondary structure from the crystal structure is indicated above the alignment. All amino acid exchanges in *B. subtilis* DivIVA that were carried out in this study are shown below. The activity of these mutant alleles was tested based on their ability to restore sporulation and cell length of a Δ*divIVA* null mutant. (+): sporulation and cell length as in wild type, (−): as in the Δ*divIVA* strain. For a complete list of mutants and phenotypes see Supplementary Table S5. (**B**) Cell morphology of Δ*divIVA* mutants carrying ectopic versions of *divIVA* with single amino acid exchanges that result in inactive proteins. Pictures were taken in mid-log growth phase (top left panel). F17A was used as an inactive mutant for the subsequent biochemical and structural work and was tested separately and essentially produces the same phenotype as F17G (bottom left panel). Right: sporulation of the same set of strains on NA agar plates. Sporulation is indicated by the dense, white appearance, whereas lack of sporulation results in cell lysis and a translucent appearance. (**C**) Localization of DivIVA-GFP with loss of function mutations in the N-terminal domain ectopically expressed in a Δ*divIVA* background (top). Bottom: F17A, used for subsequent experiments, was tested separately and produces the same phenotype as F17G. (**D**) Bacterial two-hybrid analysis of the dimerization activity of mutant alleles of the DivIVA N-terminal domain (residues 1–61). The N-terminal domain on its own produces a positive signal, presumably because of dimerization and various mutants do disrupt this interaction. F17G does not.
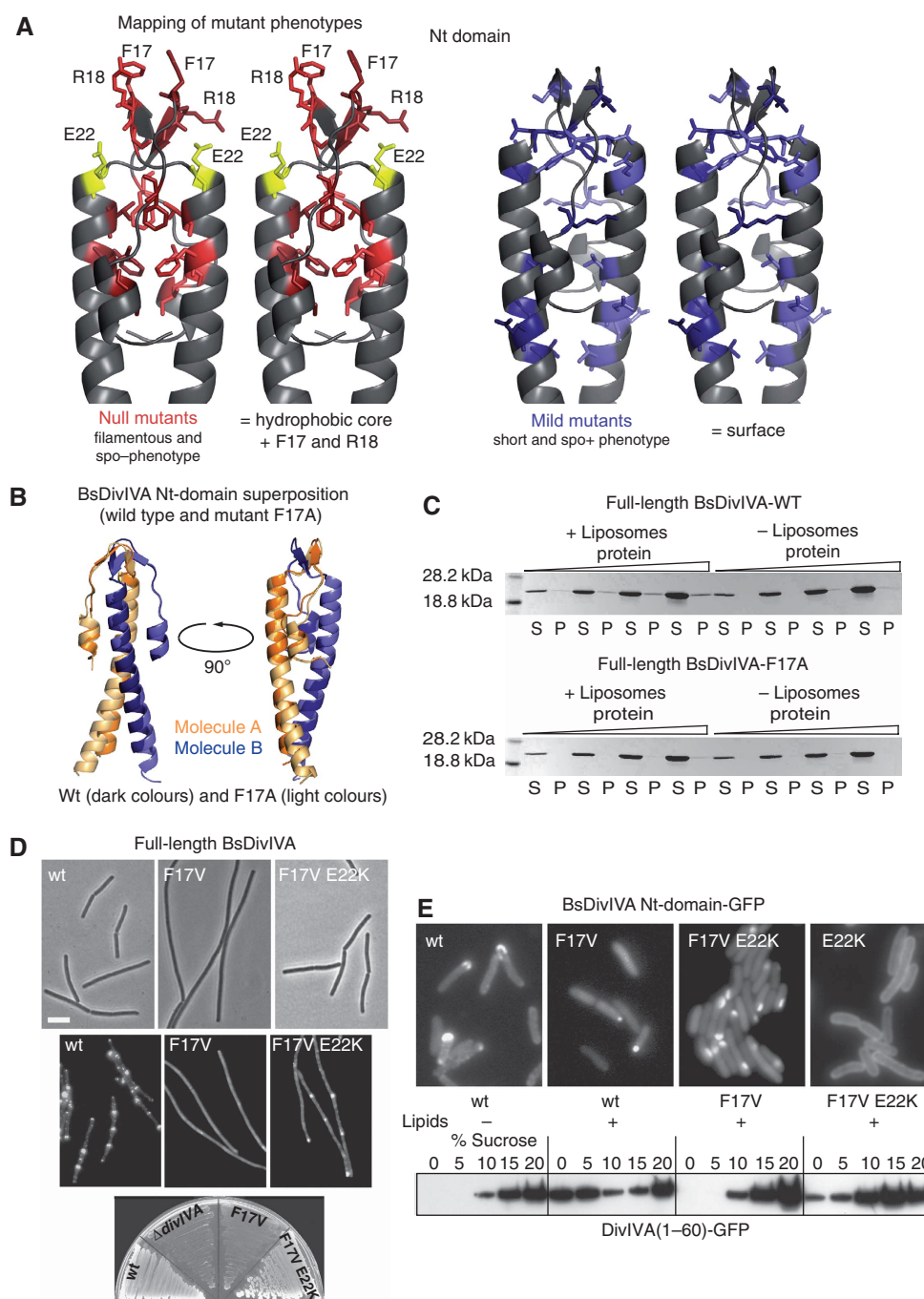
Figure 4 Residues in the crossed loops of the N-terminal domain of DivIVA are required for membrane association. (**A**) Mapping of mutant phenotypes onto the crystal structure of the N-terminal domain. Left: strong mutants that do not complement a *divIVA* knockout and do not localize to the membrane. These residues are mostly located within the hydrophobic core of the domain and are most likely folding mutants that disrupt correct formation of the molecule. Two important exceptions are F17 and R18, two amino acid residues that are exposed to the solvent within the crossed-loop structure. Right: milder mutants are mostly located on the surface. E22K (yellow) is the suppressor of F17V (see **D**, **E**). (**B**) Superposition of the F17A mutant crystal structure and the wild-type structure. We were concerned that mutating F17 to alanine would disrupt formation of the crossed loop. The superposition shows that F17A is largely unaffected. (**C**) Top: spin assay showing the interaction of DivIVA with liposomes. Bottom: same experiment using the F17A mutant. No interaction can be seen in the case of the F17A mutant. We conclude that the exposed phenylalanine residues are important for membrane interaction. (**D**) An intragenic suppressor mutation that restores localization and activity of DivIVAF17V. Top: cell morphology of Δ*divIVA* strains carrying ectopic versions of *Pspac-divIVA*. Middle: localization of ectopic versions of mutated DivIVA-GFP (Δ*divIVA* background). Bottom: sporulation of the same set of strains on NA agar plates. See Figure 3B for explanation. (**E**) Membrane localization studies of the E22K suppressor. Top: localization of Nt-domain-GFP fusions when expressed in *E. coli* DH5α. By doing this in *E. coli*, we can reduce the risk that DivIVA interacts with proteins on the membrane instead of the membrane itself. Bottom: lipid binding of Nt-domain-GFP *in vitro*. Mixtures of Nt-domain-GFP with and without lipid vesicles were centrifuged through a sucrose gradient (0–20%). Fractions were analysed by western blotting using an anti-GFP antiserum. Liposomes are enriched in the top two fractions (0–10% sucrose). Please note that lipid binding of the N-terminal domain alone requires it being fused to GFP (compare with the negative result for untagged protein in Supplementary Figure S2), presumably because of GFP's tendency to dimerize, mimicking the effect of the C-terminal domain of DivIVA.

respectively. Strain BSN54 was subjected to NTG mutagenesis, and we screened roughly 100 000 colonies. A number of colonies showed a restored sporulation phenotype, but only one displayed a restored DivIVA localization, as well. It turned out that this clone had acquired the mutation E22K in the *Pspac* driven *divIVAF17V*. When the (F17V, E22K) double mutant of *divIVA* was tested for the ability to functionally complement the *divIVA* mutant, both the sporulation and division frequency were restored back to wild-type levels (Figure 4D, top and bottom). The E22K mutation was also found to be sufficient to restore the localization pattern of DivIVAF17V-GFP (Figure 4D, middle). This suggests that the substitution of a negatively charged amino acid (glutamate) by a positively charged amino acid (lysine) at position 22 restores membrane binding of the F17V mutant protein.

It has been shown earlier that the Nt part of DivIVA fused to GFP localizes to the cell membrane in *E. coli*. Using *E. coli*, the chance that any other factors from *B. subtilis* are involved is reduced (Lenarcic *et al*, 2009). When expressed in *E. coli*, the E22K mutation restores membrane binding of a DivIVA(1–60)F17V-GFP fusion and even increases that of the wild-type variant (Figure 4E, upper panel).

To test the lipid-binding activity of the (F17V, E22K) double mutation directly, we purified DivIVA(1–60)-GFP and the F17V and (F17V, E22K) mutant variants as Ct Strep-tag fusions. The lipid-binding properties of the purified proteins were analysed in a flotation experiment using a sucrose gradient. As shown in Figure 4E, lower panel, DivIVA (1–60)-GFP remains in the bottom fraction of the gradient when no lipid vesicles are present. When mixed with lipid vesicles, the fusion protein floats to lower sucrose densities where the liposomes accumulate (Figure 4E, bottom). In contrast to this, the F17V variant remains in the bottom fraction, whereas the (F17V, E22K) mutant protein shows again lipid-binding activity, and emerges in the liposome-containing gradient fractions. This finding confirms that the E22K mutation restores lipid binding of the F17V mutation, suggesting that positive charges are involved in this activity. It is noteworthy mentioning that in this assay isolated Nt domains presumably bind to liposomes mediated by the fused (dimerizing) GFP as in another assay (Supplementary Figure S2), an untagged version of the Nt domain does not co-pellet with liposomes. The conclusion we draw here, that E22K rescues F17V *in vitro*, is unaffected by this discrepancy.

Low-resolution structure of the Ct domain reveals a coiled-coil tetramer

We also obtained crystals of the Ct domain of *B. subtilis* DivIVA described above (residues 66–164, Figure 1C). Because all crystals had very high solvent contents (Table I), resolutions of the data sets obtained remained low, between 6 and 7 Å. Using selenomethionine-substituted protein, phases were obtained from a selenium SAD experiment, and the resulting electron density map is shown in Figure 5A, left. The crystals have a solvent content of over 80%. The experimental map clearly shows tubes of electron density that represent the helices of a coiled-coil structure, as is illustrated in Figure 5A on the right. In the crystals, the protein appears to form a large ring structure with a ring diameter of ∼280 Å. The ring is not formed by uninterrupted helices going around the perimeter but several rings are intersecting.

It is not possible to observe side chains in electron density maps at 6 Å resolution and in order to build a quasi-atomic model of the Ct domain of DivIVA, we used the position of two endogenous (M116 and M134) and a mutated third (I114M), selenium-labelled methionine to determine the orientation of the helices in the electron density map as well as the approximate position of all residues in the structure (Figure 5B). The third methionine was placed so that it would appear very close to an existing one (M116), but on the other side of the helix. That way, looking at the phased anomalous differences coming from a selenium SAD experiment, we could unambiguously identify the three SeMet residues forming a triangle. Two triangles were found per asymmetric unit, and crystal symmetry produces a tetramer with four triangles, as is shown in Figure 5B. All remaining residues of the structure were placed manually by fitting an idealized α-helix with the DivIVA Ct domain I114M sequence so that the three Met residues are in the correct position. The resulting structure was not refined because of low resolution.
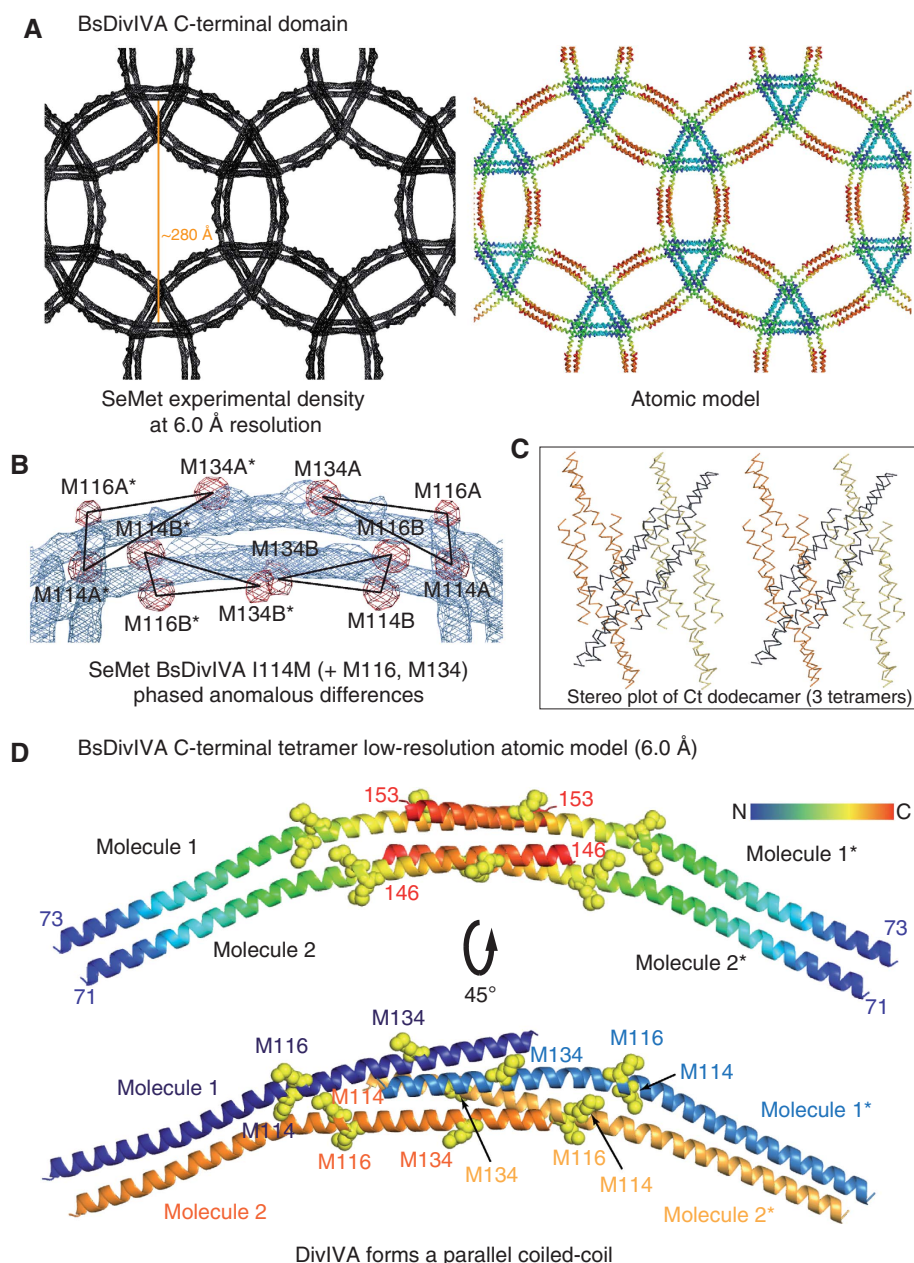
The interface between the four helices holding the tetramer together is by far the largest contact present in the structure, and is in good agreement with the ultracentrifugation data both of the full-length protein and the isolated Ct domain that we found to be mostly tetrameric (Figure 1D). The tetramer consists of two coiled-coil segments, joined at the Ct ends, to produce a short four-helix bundle (Figure 5D). The segments that form the four-helix bundle are the last residues being well conserved in the sequence alignment (which can be seen in Figure 1B, residues 127–150). The low-resolution electron density map indicates that residues ∼72 to ∼150 are ordered in the crystals. Importantly, the coiled-coil segments are parallel, with all four N-termini of the Ct domain tetramer residing at the two opposite ends of the molecule (Figure 5D).

A second crystal form (Table I) of the Ct domain was solved using tantalum bromide clusters ($Ta_6Br_{12}^{2+}$) and a tantalum SAD experiment. The resulting electron density map, again at a low resolution of 7 Å, shows the same central four-helix bundle region of the structure, only (presumably due to disorder of the remainder of the molecule). Three stacked tetramers then form a dodecamer of DivIVA molecules (Figure 5C). This finding might be relevant because of the ultracentrifugation experiments (Figure 1D) that showed 10-mers of the Ct domain.

Discussion

By separating the protein into two domains, we were able to crystallize the Nt and Ct domains of *B. subtilis* DivIVA. Combining both domains provides a composite model of *B. subtilis* full-length DivIVA (Figure 6A). The crystal structure of the Nt domain describes residues 3–52 and the low-resolution structure of the Ct domain contains information about residues ∼72 to ∼150. Both structures contain a parallel coiled-coil, and we can therefore join the two structures, resulting in a fairly extended tetramer that spans around 30 nm. We have little information about the region between the two domains. The sequence alignments show strong conservation in this region, potentially indicating a structured region (Figure 1B). We would argue against this based on two observations: the sequences inserted between residues 65 and 66 in bacterial species other than *B. subtilis* are clearly not ordered with proline-rich and glutamine-rich
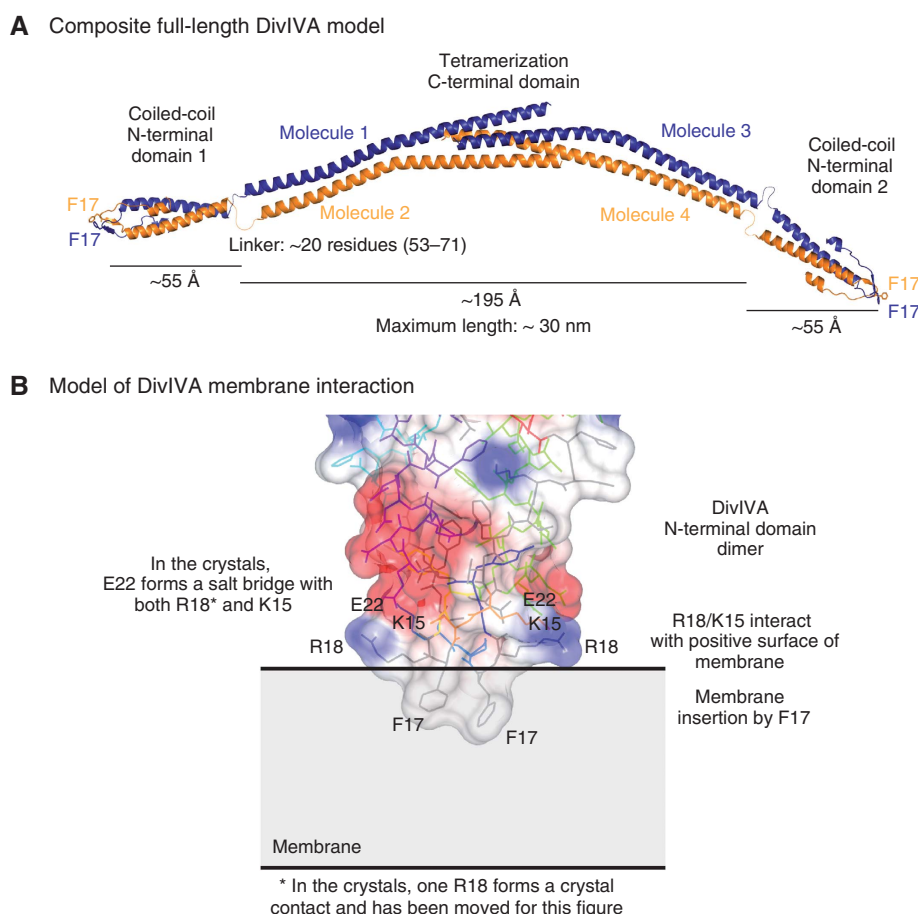
A BsDivIVA C-terminal domain

SeMet experimental density
at 6.0 Å resolution

Atomic model

B SeMet BsDivIVA I114M (+ M116, M134)
phased anomalous differences

C Stereo plot of Ct dodecamer (3 tetramers)

D BsDivIVA C-terminal tetramer low-resolution atomic model (6.0 Å)

DivIVA forms a parallel coiled-coil

Figure 5 Low-resolution X-ray crystal structures of the C-terminal domain of DivIVA. (**A**) Left: experimental, solvent-flattened electron density map of the C-terminal domain, SAD-phased with selenomethionine. The crystals have very high solvent content ($>80\%$) and diffract to only 6 Å. The electron density map shows large rings with a diameter of ~ 280 Å, which consist of tubes of electron density. Right: α-helical interpretation of the electron density map in A. The rings are not continuous because they intersect. (**B**) Determining the orientation and position of the sequence within the low-resolution electron density tubes. A mutant of CtDivIVA was prepared (I114M) that shows unambiguously four triangles (shown in black) of three selenium positions after performing a SAD experiment. The positions of the methionines allow accurate placement of idealized helices into the otherwise featureless density tubes and yield determination of the orientation of the sequence (parallel coiled-coil). (**C**) Tantalum bromide-phased ($Ta_6Br_{12}^{2+}$) low-resolution model of a second crystal form of the C-terminal domain of DivIVA. The packing shows three stacked tetramers that are similar to the ones shown in Figure 1D. The dodecamer might relate to the oligomers shown in Figure 1D, middle. (**D**) Low-resolution model of the C-terminal domain of DivIVA, as determined by the SeMet phasing and sequence determination as described in (**A**, **B**). The protein forms a tetramer from two parallel coiled-coil dimers, joined in the middle through an antiparallel four-helix bundle. Top: coloured as a rainbow from N-terminus (blue) to C-terminus (red), highlighting the parallel nature of the coiled-coils. Bottom: coloured according to chain identity, highlighting the tetramer.

repeats. The second observation relates to the NMR experiments, showing that the residues after 57 (up to 65) are not structured (Figure 2B). We conclude that there is likely a flexible linker between the N- and Ct domains, and that in the case of *B. subtilis*, the linker contains around 20 residues. Because the composite DivIVA structure is essentially

bi-functional, with two lipid-binding activities, one positioned at each end, the protein can cross-link two membranes, and this behaviour is well documented for DivIVA (Lenarcic *et al*, 2009) (Supplementary Figure S3, model I).

Using cryo-negative staining electron microscopy and a mutant DivIVA protein, Stahlberg *et al* (2004) have shown

A Composite full-length DivIVA model

B Model of DivIVA membrane interaction

* In the crystals, one R18 forms a crystal
contact and has been moved for this figure

Figure 6 How does DivIVA bind to membranes? (**A**) A composite model made from the crystal structures of the N- and C-terminal domains of *B. subtilis* DivIVA, as reported here. The domains can be unambiguously joined because they are both parallel coiled-coils. The linker region (of about 20 residues) is likely flexible (as deduced from the NMR data, Figure 2B). Overall length is ~30 nm when fully extended but if the linkers are flexible, the N-terminal domains could swing around, producing kinked and shorter conformations. Note F17 and R18, important for membrane binding, which are exposed at the two tips of the molecule. This finding and the curvature are somewhat reminiscent of eukaryotic BAR domains (shown in Supplementary Figure S1), although it is possible that the curvature shown for DivIVA is in fact induced by crystal packing. (**B**) Model of the interaction of the N-terminal domain with membranes. As only full-length DivIVA binds to membranes, and not the isolated N-terminal domains, the interaction is expected to be quite weak and to require at least two of the membrane insertions shown on the same molecule or oligomeric assembly. F17, shown here to be essential for membrane association of DivIVA, is proposed to insert into the hydrophobic core of the membrane. This then brings R18 (and K15), also essential for membrane interaction, close to the negatively charged membrane surface, enhancing affinity. Our E22K suppressor mutation of F17V can be explained with this model: it enhances the charge interaction to the point where the loss of hydrophobicity going from Phe to Val is compensated for. Please note that for this figure, the position of one R18 has been modified to form a salt bridge with E22 (as it does in the other molecule of the dimer), as it forms a crystal contact with a neighbouring molecule in the crystal structure.

that *B. subtilis* DivIVA oligomers form 'bone-like' structures. These elongated structures are about 22 nm in length and at both extremities bifurcate into two short extensions roughly 1–2 nm in length. The composite DivIVA structure of Figure 6A shows dimensions similar to that. However, to fulfil the symmetry of the bone structures, it would mean that these structures are formed by aligning at least two of the composite DivIVA structures, thus forming an octamer. Fittingly, based on sedimentation and gel filtration experiments, it was proposed that the bone-like structures contain 6–8 DivIVA monomers (Stahlberg *et al*, 2004). Stahlberg *et al* used a DivIVA G162K mutant for their experiments, and the mutation is located at the extreme C-terminus next to the tetramerization domain. Possibly, this mutation stimulates the interaction between DivIVA tetramers resulting in the bone-like structures since here we observed only tetramers formed by DivIVA. The fact that Stahlberg *et al* observed

essentially straight molecules might indicate that the coiled-coil backbone of DivIVA is flexible.

Earlier, it has been proposed that the α-helix spanning amino acids 22–41 was the membrane targeting domain of DivIVA, based on its amphipathic nature and the fact that mutations in this domain destroyed membrane binding (Lenarcic *et al*, 2009). We show here with the crystal structure of the Nt domain in combination with extensive mutagenic analyses that this suggestion was most likely incorrect. Fittingly, using the latest prediction algorithm, no amphipathic in-plane membrane targeting helix could be detected in DivIVA (Sapay *et al*, 2006). We now show that the Nt domain of DivIVA forms a remarkable crossed-loop structure whereby one monomer loops tightly over the other monomer, exposing two phenylalanine residues (F17). Mutations in these residues abolish membrane binding, and it is likely that these residues insert into the hydrophobic core of the

membrane. Our suppressor mutagenesis study shows that electrostatic interactions have a pivotal function in membrane interaction, and we predict that two neighbouring arginine residues (R18) compensate the strong negative charge on the surface of the lipid bilayer, possibly in conjunction with K15. On the basis of these data, a model emerges in which both insertion of hydrophobic residues into the membrane interior and charged interactions with the negatively charged membrane surface contribute to DivIVA's membrane-binding activity (Figure 6B). Surprisingly, F17 is not strictly conserved across even closely related species, and in fact, the central sequence of the crossed loops (residues 16–19) is less conserved than other parts of the protein (not shown). However, a closer inspection of sequence alignments shows that the loop can have different lengths, and residues F17 and R18 are invariably replaced by a different pair of hydrophobic and basic residues; F can be M or L and R is often replaced with K.

When we tested the Nt domain for lipid binding with a liposome spin assay, we could not detect any protein in the liposome pellet (Supplementary Figure S2). This was surprising as the Nt domain fused to GFP showed a clear membrane affinity both *in vivo* as well as *in vitro* (Figure 4E; Lenarcic *et al*, 2009). It is known that GFP has a tendency to form dimers (Zacharias *et al*, 2002), and the GFP moiety might tetramerize the protein and therefore increase the lipid-binding affinity. Supporting this idea, we noted that fairly high expression levels are needed to obtain membrane localization of the DivIVA(1–60)-GFP fusion in cells. This would mean that the Ct tetramerization domain of DivIVA is required for effective membrane binding, presumably because each Nt domain does not provide enough binding energy on its own for effective membrane localization.

In an earlier study, it has been argued that a specific sensing of curved membranes by individual DivIVA molecules is not a necessity (and not likely given the dimensions of a cell compared with DivIVA) to accumulate at negatively curved membranes (Lenarcic *et al*, 2009). Monte Carlo simulations showed that the long-elongated shape and bi-functional nature of DivIVA oligomers, together with the propensity to cluster, is in theory sufficient to bind to negatively curved membranes. In this 'molecular-bridging model', it is essential that DivIVA oligomers mutually interact, and this was shown earlier (Stahlberg *et al*, 2004). In their EM images, the bone-like structures are stacked end-to-end and form large lattices. This would suggest that the Nt domain of DivIVA is also involved in the interaction with other DivIVA oligomers. A tempting idea is that the exposed hydrophobic F17 residues would make the contacts; however, we have found no evidence for these interactions in our studies.

The crystal structure of the Ct tetramerization domain compels us to consider an alternative option for the binding of DivIVA to negatively curved membranes, since the DivIVA tetramer takes on a curved appearance. We think it possible that the DivIVA curvature is induced solely by crystal contacts but as it is, at least superficially, it resembles the crescent shape of eukaryotic BAR domains (Peter *et al*, 2004). BAR domains bind to curved membranes and also introduce curvature. They are generally found at the interface between the actin cytoskeleton and lipid membranes, and are involved in vesicle formation and membrane remodelling. Several different versions exist that bind to positively (outside of vesicles, BAR, F-BAR, N-BAR) and also negatively (inside of vesicles, I-BAR) curved membranes (review Frost *et al*, 2009). They achieve this by having structures that position charged lipid-binding regions onto a curved backbone (Supplementary Figure S1). The curved backbone and the occurrence of lipid interactions at the tips of the DivIVA tetramer show similarities with BAR domains (Saarikangas *et al*, 2009). Possibly, the middle, curved part of DivIVA contains positive-charged residues at the concave side that bind to the membrane through charged interactions with phospholipid head groups (Supplementary Figure S3, III), thus preferring to bind to negatively curved membranes. Because our structure of the Ct domain is of low resolution, with the positions of side chains uncertain, it is impossible to be sure about the electrostatic potential at its surface. It should be mentioned that we were unable to detect any affinity of purified Ct DivIVA for liposomes, but the interactions between this isolated domain and lipid bilayers might be too weak to detect without the additional Nt domains providing binding energy. In this respect, it is interesting to note that *in vitro* the addition of DivIVA to liposomes does not result in grossly perturbed structures, a clear difference to BAR domains that bind to negatively curved membranes. Moreover, as can be seen easily from the mismatch of curvatures in Supplementary Figures S3 and S4, a BAR-like mechanism is unlikely, simply because the curvature of the membrane is so small. Clearly, we need more information on the structure of DivIVA in contact with lipid bilayers to resolve the mechanism of binding to curved membranes. Hopefully, knowledge of the molecular structure and the identification of the primary membrane-association sites at the tips of the elongated molecule will guide us to a complete understanding of lipid and protein interactions of DivIVA.

Materials and methods

Protein expression and purification

Full-length *B. subtilis* DivIVA (BsDivIVA, UNI_PROT ID: DIV4A_BACSU, residues 1–164) with and without His$_6$ tag, His$_6$-tagged Nt domain *B. subtilis* DivIVA-1 (NtDivIVA-1-GSHHHHHH, residues 1–65), untagged NtBsDivIVA-2 (residues 1–57) and Ct domain *B. subtilis* DivIVA-His$_6$ (CtDivIVA-GSHHHHHH, residues 66–164) were cloned into the NdeI and BamHI sites of pHis17 (Bruno Miroux, MRC-LMB, personal communication). PCR mutagenesis generated mutants BsDivIVA-F17A and NtDivIVA-F17A, respectively. The same method was used for the generation of CtDivIVA-I114M-GSHHHHHH, using pHis17-CtDivIVA-His as template. All non-labelled proteins were expressed in *E. coli* C41 cells (Miroux and Walker, 1996), which were induced at OD$_{600}$ 0.6 by the addition of 1 mM IPTG. Cells were opened by sonication. Untagged proteins were purified by anion exchange chromatography using a HiTrapQ HP column (GE Healthcare) followed by size exclusion chromatography on a Sepahcryl S100 column (GE Healthcare) in 20 mM Tris–HCl, 200 mM NaCl, 1 mM EDTA, 1 mM sodium azide, pH 8.0 for BsDivIVA or the same, pH 8.5 for BsDivIVA-F17A or the same buffer with 50 mM NaCl and pH 7.5 for NtDivIVA-2 and NtDivIVA-F17A. Only the BsDivIVA purification included a 30% (saturation) ammonium sulfate precipitation step before anion exchange chromatography. His-tagged proteins were purified by HisTrap nickel-affinity chromatography (GE Healthcare) followed by size exclusion chromatography on a Sephacryl S100 column in 20 mM Tris–HCl, 200 mM NaCl, 1 mM EDTA, 1 mM sodium azide, pH 8.0 for BsDivIVA-His$_6$ and CtDivIVA-His$_6$ or 20 mM Tris–HCl, 50 mM NaCl, 1 mM EDTA, 1 mM sodium azide, pH 7.5 for NtDivIVA-1-His$_6$. Fractions containing pure protein were concentrated using spin concentrators and stored frozen at −80°C.

CtDivIVA-I114M-His$_6$ was expressed in *E. coli* BL21-AI cells (Invitrogen). For expression of selenomethionine-substituted protein in non-methionine auxotrophic, *E. coli* cells were grown as described earlier (van den Ent *et al*, 1999). A culture in exponential growth phase was induced over night at 20°C by the addition of 0.2% arabinose. The protein was purified as for CtDivIVA-His$_6$ but all buffers included fresh 5 mM β-mercaptoethanol or 5 mM DTT for the last step. Fractions containing protein were concentrated in spin concentrators and stored frozen at −80°C.

For NMR experiments, two isotopically labelled His$_6$-tagged NtDivIVA-1 proteins were made, both using M9 minimal media supplemented with minerals and vitamins as described above. For ^{15}N-labelling, media contained 20 mM [^{15}N]NH$_4$Cl, and for ^{13}C-^{15}N double-labelling, media contained 20 mM [^{15}N]NH$_4$Cl and 0.04% (w/v) [^{13}C]-glucose and 0.36% (w/v) [^{12}C]-glucose. The proteins were purified as described above from a 1.8 l culture.

DivIVA(1–60)-Strep, and its F17V and (F17V, E22K) mutant variants were overexpressed in *E. coli* BL21(DE3) using the expression plasmid pSH139, pSH161 and pSH162, respectively. Expression was induced by the addition of 1 mM IPTG to exponentially growing cultures, and the proteins were purified using Streptactin Sepharose (IBA, Göttingen, Germany). After purification, protein-containing fractions were pooled and aliquots were stored at −80°C.

Crystallization and structure determination

All crystals were grown at 19°C using the sitting-drop vapour-diffusion technique and initial hits were found using our in-house nanolitre crystallization facility (Stock *et al*, 2005). Data were integrated and reduced using MOSFLM and SCALA (CCP4, 1994). Crystals of NtDivIVA-2 were grown in 0.1 M Tris–HCl, pH 8.0, 0.6 M sodium formate and 29.57% (w/v) PEG 2000 MME. Crystals were frozen in liquid nitrogen without adding any extra cryoprotectant. High-resolution X-ray diffraction data were collected at beamline ID29, ESRF, Grenoble, France. The crystal structure was solved by single anomalous dispersion using a quick-soak NaI derivative (Table I). The coordinates of eight sites from the NaI derivative were determined using SHELXCD (Sheldrick, 2008). SAD phases were calculated using PHASER 2.1 (McCoy *et al*, 2007). A rough model was then refined using REFMAC5 (Murshudov *et al*, 1997), the structure was manually completed in MAIN (Turk, 1992) and water molecules were added using ARP/wARP (Langer *et al*, 2008).

Crystals of NtDivIVA-F17A were grown in 0.2 M sodium acetate, pH 4.0 and 27.14% (w/v) PEG 3000 and frozen in liquid nitrogen after equilibration in a solution containing mother liquor plus 20% (w/v) of ethylene glycol. X-ray diffraction data were collected to 1.9 Å on a Rigaku RU-300 rotating anode with a MAR Research dtb imaging plate detector. Molecular replacement was performed with NtDivIVA-2 as the search model with PHASER. The initial model was refined using simulated annealing in PHENIX (Adams *et al*, 2002), which was also used for water picking. Several cycles of refinement and iterative model building with MAIN were carried out.

Crystals of CtDivIVA-I114M-His$_6$ were grown in 0.179 M HEPES, pH 7.0, 1.82 M ammonium formate and frozen in liquid nitrogen from a solution containing mother liquor plus 25% of glycerol. Data collection was performed on beamline id14eh4, ESRF, Grenoble, France (Table I). Phasing was done by single anomalous dispersion using the peak wavelength of selenium. The coordinates of six sites were determined using SHELXCD and were used for phasing using PHASER 2.1.

Crystals of CtDivIVA-His$_6$ grown in 0.1 M imidazole pH 7.0, 0.345 M Li$_2$SO$_4$ and 9.2% PEG 3000 were dehydrated by adding 15% of ethylene glycol in the reservoir solution and were then kept for 1 month at 4°C. Then, the crystals were soaked over night in a highly concentrated solution of Ta$_6$Br$_{12}^{2+}$ (dark green) at 4°C and frozen in liquid nitrogen from a solution containing mother liquor plus 30% ethylene glycol. Data collection was performed on beamline IO2 at Diamond, Harwell, UK. Phasing was done by single anomalous dispersion using the peak wavelength of tantalum (L III, 1.2548 Å). The coordinates of five sites were determined using SHELXCD and were used for SAD phasing using PHASER 2.1.

Analytical ultracentrifugation: sedimentation-equilibrium experiments

Sedimentation-equilibrium experiments were performed in a Beckman Optima XLI analytical ultracentrifuge with a Ti-60 rotor using interference and absorbance at 280 and 230 nm at 25°C. The proteins were loaded into six-sector 12 mm path length cells at three different concentrations. Samples of BsDivIVA were dialysed against 20 mM Tris–HCl, 1 mM EDTA, 300 mM NaCl, pH 7.5 and then diluted to 4.6, 1 and 0.2 mg/ml. NtDivIVA-1-His was dialysed against 20 mM Tris–HCl, 1 mM EDTA, 300 mM NaCl and 25 mM phosphate buffer, pH 6.8. CtDivIVA-His$_6$ was dialysed against 20 mM Tris–HCl, 1 mM EDTA, 200 mM NaCl, pH 7.5. Both were then diluted to 10, 1.5 and 0.2 mg/ml. The samples were centrifuged until they reached equilibrium as judged by the changes in the subsequent scans at speeds of 10 000, 14 000 and 20 000 r.p.m. (BsDivIVA) or 20 000, 28 000 and 40 000 r.p.m. (NtDivIVA-1-His and CtDivIVA-His). Data were analysed using UltraSpin software (http://ultraspin.mrc-cpe.cam.ac.uk).

NMR experiments and assignment

The proteins were dialysed against buffer containing 25 mM sodium phosphate, pH 6.8 and then diluted to 1 mM for NMR experiments. All NMR spectra were recorded on a Bruker DRX-600 spectrometer. 2D ^{15}N-HSQC and 3D HNCA, HNCOCA, HNCACB, CBCACONH, HNCO and HNCACO spectra of NtDivIVA-1-His were recorded at 293°K. Spectra were processed with TopSpin and analysed with Sparky (Goddard, TD, Kneller, DG, SPARKY 3, University of California, San Francisco). The backbone resonances were assigned by standard triple-resonance procedures using a uniformly ^{15}N, ^{13}C-labelled sample. The empirical prediction of φ and ψ backbone torsion angles using the chemical shifts assignments for NtDivIVA-1-His was done with TALOS (Cornilescu *et al*, 1999).

B. subtilis strains and methods

The *B. subtilis* strains used in this study are listed in Supplementary Table S6. Routinely, cells of *B. subtilis* were cultivated either in Luria Bertani broth or on nutrient agar plates. If necessary, antibiotics and additional supplements were added at the following concentrations: spectinomycin (50 µg/ml), tetracyclin (10 µg/ml), IPTG (1 mM) or xylose (0.5%). Transformation of *B. subtilis* was done as described earlier (Hamoen *et al*, 2002). To visualize DivIVA(1–60)-GFP-Strep proteins by immunostaining, we used a polyclonal rabbit antiserum recognizing GFP (Marston *et al*, 1998).

Plasmid and strain construction

Plasmid pSH2 contains the *B. subtilis divIVA* gene under control of the IPTG inducible *Pspac* promoter. For its construction, a DNA fragment comprising the ribosomal binding site and the open reading frame of the *divIVA* gene was PCR amplified from wild-type genomic DNA. The obtained DNA fragment was cut using *Bam*HI/*Sac*I and ligated with plasmid pAPNC213. Plasmid pSH34 was obtained in the same way, but with genomic DNA from BSN57 as the template. The introduction of single amino acid exchanges into the *divIVA* gene (present on plasmid pSH2), the *divIVA-gfp* gene (present on plasmid pDG9, or alternatively, pSH3) or into *divIVA$^{1–180}$-gfp* (present on plasmid pDG15) was carried out using the modified Quickchange mutagenesis protocol (Zheng *et al*, 2004). All mutant derivatives of plasmid pSH2 were transformed into *B. subtilis* 168 and spectinomycin-resistant clones were analysed by PCR whether the plasmid had been inserted into the *aprE* locus by double crossover. In a second transformation, these strains were combined with the Δ*divIVA*::*tet* allele (strain 4041). Similarly, mutant derivatives of plasmids pDG9 (*Pxyl-divIVA-gfp*) and pSH3 (*Pxyl-divIVA-gfpA206K*) were inserted into the *amyE* locus of *B. subtilis* 168 and amylase negative clones were selected based on iodine staining of starch containing agar plates. The native *divIVA* locus of these strains was then replaced by the Δ*divIVA*::*tet* allele in a second transformation. Where necessary, the spectinomycin-resistant cassette was replaced by the kanamycin/neomycin resistance gene of plasmid pVK73 by double homologous recombination.

An Nt fragment of the *divIVA* gene comprising the first 61 amino acids was obtained by PCR from genomic DNA. The DNA fragment was cut *Xba*I and *Kpn*I and ligated with pUT18, pUT18C, pKT25 and p25-N. Mutant variants of these constructs were obtained in a similar way but with pPD24 (I8A), pPD26 (F13A), pPD28 (F17G), pPD30 (V25A) and pPD35 (L29A) plasmid DNA as the templates in the PCR reaction.

For the expression of a DivIVA(1–61)-Strep, an appropriate *divIVA* fragment was created with a Ct Strep-tag. This fragment was digested by *Nde*I and *Bam*HI and ligated to pET11a to give plasmid pSH91.

To fuse DivIVA(1–60)-GFP to a Ct Strep-tag, a suitable *divIVA*$^{1-180}$-*gfp* fragment was amplified from plasmid pDG15, cut *Nde*I, ligated to pSH105 (which is a pET11a derivative expressing GFP-Strep), and named pSH139. For the overexpression of F17V and F17V E22K mutants thereof, plasmids pSH161 and pSH162 were constructed. DNA fragments encoding the corresponding genes were obtained by PCR from plasmids pSH17 and pSH152, cut *Nhe*I/ *Bam*HI, and ligated to plasmid pET11a.

Bacterial two-hybrid analysis
To determine dimerization activity of the DivIVA Nt domain, the bacterial two-hybrid system was used (Karimova *et al*, 1998). Plasmids encoding Nt fusions of this domain with the T18 or the T25 fragment of the *Bordetella pertussis* adenylate cyclase were co-transformed in *E. coli* BTH101. Transformants were selected on NA agar plates containing ampicillin (100 µg/ml), kanamycin (50 µg/ml), X-Gal (0.004%) and IPTG (0.1 mM), and photographs were taken after 40 h of growth at 30°C.

Suppressor screen
N-methyl-N^9-nitro-*N*-nitrosoguanidine (NTG) mutagenesis was carried out according to a standard protocol (Harwood and Cutting, 1990). Briefly, BSN54 cells were grown in PAB medium to mid-log growth phase, washed in 10 ml SC buffer (0.15 M NaCl, 0.01 M sodium citrate, pH 7.0) and treated with 50 µg/ml NTG for 30 min at 37°C. Subsequent to mutagenesis, cells were washed two more times and finally plated on nutrient agar plates containing 1 mM IPTG. Plates were left several days at 37°C, and spo$^+$ suppressors were selected based on their brownish appearance on a background of lysing and thus translucent spo$^-$ colonies.

Liposome sedimentation assays
Initially, lipids from Avanti Polar Lipids (*E. coli* total extract or *E. coli* polar extract) were diluted to 25 mg/ml in chloroform. Then, 1 mg of lipid was diluted into a 1:3 mix of chloroform:methanol, desiccated with a gentle flow of nitrogen to create a thin lipid film and further desiccated for 1 h under vacuum. Liposomes were made by resuspension of the lipid film in 25 mM Tris–HCl, 150 mM NaCl, pH 7.5 to a final concentration of 1 mg/ml. Finally, liposomes were sized by extrusion using a 1-µm membrane filter. For sedimentation assays, protein and liposomes were mixed at different concentrations in the assay buffer to a final volume of 100 µl. A measure of 0.15 mg/ml of NtDivIVA-His and CtDivIVA-His were titrated with 0.05, 0.1, 0.15, 0.25 and 0.5 mg/ml of liposomes. A measure of 0.15 mg/ml of BsDivIVA was titrated with 0.05, 0.1, 0.15, 0.20, 0.25 and 0.5 mg/ml of liposomes. A measure of 0.05 mg/ml of liposomes were titrated with 0.05, 0.15, 0.25 and 0.5 mg/ml of BsDivIVA and BsDivIVA-F17A. After incubation at room temperature for 25 min, samples were centrifuged at 65 000 r.p.m. for 10 min in a Beckman TLA100 rotor. Supernatants were removed immediately and pellets were resuspended in an equal volume of buffer. Samples from supernatant and pellet were subjected to SDS–PAGE and visualized by PAGE blue stain.

Liposome flotation assays
Liposomes were prepared as described by Avanti Polar Lipids. Liposomes were mixed with binding buffer (20 mM Tris/HCl pH 7.5, 200 mM KCl, 2 mM MgCl$_2$, 0.3 mM DTT and 1 mg/ml BSA) and freeze-thawed several times followed by extrusion through a 0.4-µm pore size filter (Avanti Polar Lipids, Inc). For lipid binding, 1.5 µg of the respective DivIVA(1–60)-GFP-Strep protein was mixed with 50 µg of lipids in a total volume of 100 µl of binding buffer also containing a protease inhibitor cocktail (Roche). After 10 min at room temperature, the samples were titrated to a final sucrose concentration of 20%, overlaid by a discontinuous sucrose gradient (15, 10, 5, 0%) and then centrifuged for 2 h in an MLS50 swing out rotor at 25 000 r.p.m. After centrifugation, the gradient was fractionated and analysed by western blot.

Supplementary data
Supplementary data are available at *The EMBO Journal* Online (http://www.embojournal.org).

Conflict of interest

The authors declare that they have no conflict of interest.

References

Adams PD, Grosse-Kunstleve RW, Hung LW, Ioerger TR, McCoy AJ, Moriarty NW, Read RJ, Sacchettini JC, Sauter NK, Terwilliger TC (2002) PHENIX: building new software for automated crystallographic structure determination. *Acta Crystallogr D Biol Crystallogr* **58:** 1948–1954

Ben-Yehuda S, Rudner DZ, Losick R (2003) RacA, a bacterial protein that anchors chromosomes to the cell poles. *Science* **299:** 532–536

CCP4 (1994) The CCP4 suite: programs for protein crystallography. *Acta Crystallogr D Biol Crystallogr* **50:** 760–763

Cornilescu G, Delaglio F, Bax A (1999) Protein backbone angle restraints from searching a database for chemical shift and sequence homology. *J Biomol NMR* **13:** 289–302

Edwards DH, Errington J (1997) The Bacillus subtilis DivIVA protein targets to the division septum and controls the site specificity of cell division. *Mol Microbiol* **24:** 905–915

Fadda D, Pischedda C, Caldara F, Whalen MB, Anderluzzi D, Domenici E, Massidda O (2003) Characterization of divIVA and other genes located in the chromosomal region downstream of the dcw cluster in *Streptococcus pneumoniae*. *J Bacteriol* **185:** 6209–6214

Flärdh K (2003) Essential role of DivIVA in polar growth and morphogenesis in *Streptomyces coelicolor* A3(2). *Mol Microbiol* **49:** 1523–1536

Frost A, Unger VM, De Camilli P (2009) The BAR domain superfamily: membrane-molding macromolecules. *Cell* **137:** 191–196

Gregory JA, Becker EC, Pogliano K (2008) *Bacillus subtilis* MinC destabilizes FtsZ-rings at new cell poles and contributes to the timing of cell division. *Genes Dev* **22:** 3475–3488

Hamoen LW, Smits WK, de Jong A, Holsappel S, Kuipers OP (2002) Improving the predictive value of the competence transcription factor (ComK) binding site in *Bacillus subtilis* using a genomic approach. *Nucleic Acids Res* **30:** 5517–5528

Harwood CR, Cutting SM (1990) *Molecular Biological Methods for Bacillus Subtilis*. Chichester: J Wiley

Hempel AM, Wang SB, Letek M, Gil JA, Flärdh K (2008) Assemblies of DivIVA mark sites for hyphal branching and can establish new zones of cell wall growth in *Streptomyces coelicolor*. *J Bacteriol* **190:** 7579–7583

Karimova G, Pidoux J, Ullmann A, Ladant D (1998) A bacterial two-hybrid system based on a reconstituted signal transduction pathway. *Proc Natl Acad Sci USA* **95:** 5752–5756

Langer G, Cohen SX, Lamzin VS, Perrakis A (2008) Automated macromolecular model building for X-ray crystallography using ARP/wARP version 7. *Nat Protoc* **3:** 1171–1179

Lenarcic R, Halbedel S, Visser L, Shaw M, Wu LJ, Errington J, Marenduzzo D, Hamoen LW (2009) Localisation of DivIVA by targeting to negatively curved membranes. *EMBO J* **28:** 2272–2282

Letek M, Fiuza M, Ordonez E, Villadangos AF, Flardh K, Mateos LM, Gil JA (2009) DivIVA uses an N-terminal conserved region and two coiled-coil domains to localize and sustain the polar growth in *Corynebacterium glutamicum*. *FEMS Microbiol Lett* **297:** 110–116

Lupas A, Van Dyke M, Stock J (1991) Predicting coiled coils from protein sequences. *Science* **252:** 1162–1164

Marston AL, Thomaides HB, Edwards DH, Sharpe ME, Errington J (1998) Polar localization of the MinD protein of *Bacillus subtilis* and its role in selection of the mid-cell division site. *Genes Dev* **12:** 3419–3430

McCoy AJ, Grosse-Kunstleve RW, Adams PD, Winn MD, Storoni LC, Read RJ (2007) Phaser crystallographic software. *J Appl Crystallogr* **40:** 658–674

Miroux B, Walker JE (1996) Over-production of proteins in *Escherichia coli*: mutant hosts that allow synthesis of some membrane proteins and globular proteins at high levels. *J Mol Biol* **260:** 289–298

Murshudov GN, Vagin AA, Dodson EJ (1997) Refinement of macromolecular structures by the maximum-likelihood method. *Acta Crystallogr D Biol Crystallogr* **53:** 240–255

Perry SE, Edwards DH (2004) Identification of a polar targeting determinant for *Bacillus subtilis* DivIVA. *Mol Microbiol* **54:** 1237–1249

Peter BJ, Kent HM, Mills IG, Vallis Y, Butler PJ, Evans PR, McMahon HT (2004) BAR domains as sensors of membrane curvature: the amphiphysin BAR structure. *Science* **303:** 495–499

Ramamurthi KS, Losick R (2009) Negative membrane curvature as a cue for subcellular localization of a bacterial protein. *Proc Natl Acad Sci USA* **106:** 13541–13545

Saarikangas J, Zhao H, Pykalainen A, Laurinmaki P, Mattila PK, Kinnunen PK, Butcher SJ, Lappalainen P (2009) Molecular mechanisms of membrane deformation by I-BAR domain proteins. *Curr Biol* **19:** 95–107

Sapay N, Guermeur Y, Deleage G (2006) Prediction of amphipathic in-plane membrane anchors in monotopic proteins using a SVM classifier. *BMC Bioinformatics* **7:** 255

Sheldrick GM (2008) A short history of SHELX. *Acta Crystallogr A* **64:** 112–122

Stahlberg H, Kutejova E, Muchova K, Gregorini M, Lustig A, Muller SA, Olivieri V, Engel A, Wilkinson AJ, Barak I (2004) Oligomeric structure of the *Bacillus subtilis* cell division protein DivIVA determined by transmission electron microscopy. *Mol Microbiol* **52:** 1281–1290

Stock D, Perisic O, Löwe J (2005) Robotic nanolitre protein crystallisation at the MRC Laboratory of Molecular Biology. *Prog Biophys Mol Biol* **88:** 311–327

Thompson JD, Higgins DG, Gibson TJ (1994) CLUSTAL W: improving the sensitivity of progressive multiple sequence alignment through sequence weighting, position-specific gap penalties and weight matrix choice. *Nucleic Acids Res* **22:** 4673–4680

Turk D (1992) Weiterentwicklung eines Programms für Molekülgraphik und Elektronendichte-Manipulation und seine Anwendung auf verschiedene Protein Strukturaufklärungen. PhD thesis, Technical University of Munich, Germany

van den Ent F, Lockhart A, Kendrick-Jones J, Löwe J (1999) Crystal structure of the N-terminal domain of MukB: a protein involved in chromosome partitioning. *Structure* **7:** 1181–1187

Wang SB, Cantlay S, Nordberg N, Letek M, Gil JA, Flärdh K (2009) Domains involved in the *in vivo* function and oligomerization of apical growth determinant DivIVA in *Streptomyces coelicolor*. *FEMS Microbiol Lett* **297:** 101–109

Wu LJ, Errington J (2003) RacA and the Soj-Spo0J system combine to effect polar chromosome segregation in sporulating *Bacillus subtilis*. *Mol Microbiol* **49:** 1463–1475

Xu H, Chater KF, Deng Z, Tao M (2008) A cellulose synthase-like protein involved in hyphal tip growth and morphological differentiation in *Streptomyces*. *J Bacteriol* **190:** 4971–4978

Zacharias DA, Violin JD, Newton AC, Tsien RY (2002) Partitioning of lipid-modified monomeric GFPs into membrane microdomains of live cells. *Science* **296:** 913–916

Zheng L, Baumann U, Reymond JL (2004) An efficient one-step site-directed and site-saturation mutagenesis protocol. *Nucleic Acids Res* **32:** 115